HHS Public Access

Author manuscript

ACS Chem Biol. Author manuscript; available in PMC 2017 August 03.

Published in final edited form as:

ACS Chem Biol. 2016 June 17; 11(6): 1669–1676. doi:10.1021/acschembio.6b00144.

Transition State Structure and Inhibition of Rv0091, a 5′-Deoxyadenosine/5′-methylthioadenosine Nucleosidase from *Mycobacterium tuberculosis*

Hilda A. Namanja-Magliano[†], **Christopher F. Stratton**[†], and **Vern L. Schramm**[*]

Department of Biochemistry, Albert Einstein College of Medicine, 1300 Morris Park Avenue, Bronx, New York 10461, United States

Abstract

5′-Methylthioadenosine/*S*-adenosylhomocysteine nucleosidase (MTAN) is a bacterial enzyme that catalyzes the hydrolysis of the *N*-ribosidic bond in 5′-methylthioadenosine (MTA) and *S*-adenosylhomocysteine (SAH). MTAN activity has been linked to quorum sensing pathways, polyamine biosynthesis, and adenine salvage. Previously, the coding sequence of Rv0091 was annotated as a putative MTAN in *Mycobacterium tuberculosis*. Rv0091 was expressed in *Escherichia coli*, purified to homogeneity, and shown to be a homodimer, consistent with MTANs from other microorganisms. Substrate specificity for Rv0091 gave a preference for 5′-deoxyadenosine relative to MTA or SAH. Intrinsic kinetic isotope effects (KIEs) for the hydrolysis of [1′-^{3}H], [1′-^{14}C], [5′-$^{3}H_2$], [9-^{15}N], and [7-^{15}N]MTA were determined to be 1.207, 1.038, 0.998, 1.021, and 0.998, respectively. A model for the transition state structure of Rv0091 was determined by matching KIE values predicted *via* quantum chemical calculations to the intrinsic KIEs. The transition state shows a substantial loss of C1′–N9 bond order, well-developed oxocarbenium character of the ribosyl ring, and weak participation of the water nucleophile. Electrostatic potential surface maps for the Rv0091 transition state structure show similarity to DADMe-immucillin transition state analogues. DADMe-immucillin transition state analogues showed strong inhibition of Rv0091, with the most potent inhibitor (5′-hexylthio-DADMe-immucillinA) displaying a K_i value of 87 pM.

Graphical abstract

[*]**Corresponding Author**. Phone: 718-430-2813. vern.schramm@einstein.yu.edu.
[†]These authors contributed equally to this work.

ASSOCIATED CONTENT

Supporting Information

The Supporting Information is available free of charge on the ACS Publications website at DOI: 10.1021/acschembio.6b00144.

Supporting Information Figure S1–S5 and Supporting Information Tables S1–S2; complete experimental procedures for expression and purification of Rv0091; kinetic assays and oligomeric state determination of Rv0091; synthesis of isotopically labeled MTA substrates; measurement of KIEs and forward commitment; computational analyses; and determination of inhibition constants (PDF)

The authors declare no competing financial interest.

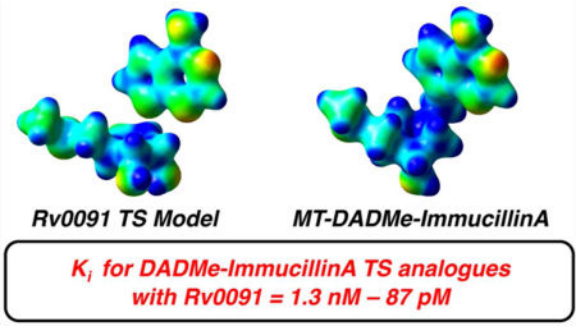

Mycobacterium tuberculosis is the causative agent of tuberculosis (TB), a leading cause of death among infectious diseases.[1] In 2014, 9.6 million cases of TB were reported, and 1.5 million people died of TB-related infections. Accordingly, the continued rise of multidrug-resistant, extensively drug-resistant, and totally drug-resistant strains of *M. tuberculosis* has become a major public health concern.[2] These challenges highlight the pressing need for new antitubercular therapies with novel targets and mechanisms of action.

5′-Methylthioadenosine/*S*-adenosylhomocysteine nucleosidases (MTANs) are involved in *S*-adenosylmethionine (SAM)-related pathways, including methylation, polyamine biosynthesis, adenine salvage, the biosynthesis of quorum sensing autoinducers and radical reactions involving SAM.[3,4] MTANs catalyze the hydrolysis of the *N*-ribosidic bond in 5′-methylthioadenosine (MTA), *S*-adenosylhomocysteine (SAH), and 5′-deoxyadenosine (5′-dAdo; Figure 1). The absence of MTANs in human metabolism makes this protein class an appealing target for antibacterials that function through blocking the quorum-sensing pathway or SAM recycling.

Previously, we reported models for the transition state (TS) structures of MTANs from *Escherichia coli*,[5] *Streptococcus pneumonia*,[6] and *Neisseria meningitidis*[7] using a combination of experimental kinetic isotope effect (KIE) measurements and computational methods. Intrinsic KIEs report on bond vibrational changes between the ground state (GS) and TS of chemical reactions and can be used as boundary constraints on quantum chemical calculations to model the structure of reactants at the TS. Such analyses provide information that can be leveraged in the design of chemically stable analogues that mimic features of the TS structure.[4,8–10] TS analogues designed for the MTAN reaction function as extremely potent inhibitors with K_d values in the picomolar (pM) and femtomolar (fM) range.[11–13] Importantly, these inhibitors have been shown to disrupt quorum sensing pathways in *E. coli* and *Vibrio cholerae*[14] and inhibit growth in *Helicobacter pylori* by blocking menaquinone biosynthesis.[15]

The Rv0091 protein from *M. tuberculosis* was annotated previously as a putative bifunctional MTA/SAH nucleosidase.[16] Herein, we report the expression, purification, and kinetic characterization of Rv0091. We demonstrate that the preferred substrate for Rv0091 is 5′-dAdo, and the protein exhibits less efficient nucleosidase activity with MTA and SAH substrates. A model of the Rv0091 TS structure for MTA hydrolysis was produced by matching KIE values predicted *via* quantum chemical calculations to a family of intrinsic

KIEs. This model reveals that the Rv0091 TS structure and DADMe-immucillin TS analogues share similar electrostatic distributions. The potential of DADMe-immucillin TS analogues to modulate Rv0091 activity was investigated *via in vitro* inhibition assays.

RESULTS AND DISCUSSION

Oligomeric State and Substrate Specificity for Rv0091

A synthetic gene was designed for Rv0091 (NCBI GenBank: CCP42816.1) and purchased from DNA2.0 Inc. in a pJexpress414 expression vector. Rv0091 was heterologously expressed in *E. coli* with an *N*-terminal His_6 tag and purified to homogeneity *via* Ni^{2+}-affinity chromatography. The purified protein was analyzed *via* SDS-PAGE to reveal a protein band of a molecular weight consistent with the predicted monomer size for Rv0091 (29.4 kDa; Figure 2). To determine the oligomeric state of Rv0091, the purified protein was treated with glutaraldehyde to enable intersubunit cross-linking.[17] SDS-PAGE analysis of the cross-linked protein revealed a band consistent with a dimeric oligomerization state (Figure 2). These data are consistent with previous reports for MTANs from other organisms, which have been characterized as homodimers in X-ray crystallography.[14,18–20]

Recently, a 5′-methylthioadenosine phosphorylase (MTAP) was identified in *M. tuberculosis*[21] and *M. smegmatis*.[22] MTAPs catalyze the phosphorolysis of MTA to adenine and 5′-methylthioribose-1′-phosphate. Prior to these reports, MTAPs were believed to be absent from bacteria, and the biological reason why *M. tuberculosis* and *M. smegmatis* expresses both MTAP and MTAN is currently unknown. We explored the substrate specificity of Rv0091 by determining the kinetic constants with MTA, SAH, and 5′-dAdo.[23] These experiments indicate that the preferred substrate for Rv0091 is 5′-dAdo, which displayed a specificity constant (k_{cat}/K_M) 7-fold greater than MTA and 700-fold greater than SAH (Table 1). MTA was reported as the preferred substrate for *M. tuberculosis* MTAP,[21] and the addition of phosphate to the Rv0091 reaction mixture did not enhance the rate of MTA hydrolysis. These data indicate Rv0091 does not exhibit MTAP activity and suggests that Rv0091 primarily functions as a 5′-dAdo nucleosidase.

The catalytic efficiencies (k_{cat}/K_M) for Rv0091 with 5′-dAdo and MTA (Table 1) are lower than those of *E. coli* MTAN ($k_{cat\text{-}MTA}/K_{M\text{-}MTA} = 2.3 \times 10^6\ M^{-1}\ s^{-1}$; $k_{cat\text{-}5'dAdo}/K_{M\text{-}5'dAdo} = 0.8 \times 10^6\ M^{-1}\ s^{-1}$).[23] The low catalytic efficiency of enzymes from *M. tuberculosis*, such as Rv0091, has been attributed to the slow doubling time of *M. tuberculosis* (24 h) as compared to *E. coli* (20 min).[24]

Determination of Intrinsic KIEs for MTA Hydrolysis

KIEs for the hydrolysis of MTA by Rv0091 were measured *via* the competitive radiolabel approach[9,10] using MTA substrates with isotopic labels incorporated at sensitive or remote positions (Table 2). Isotope effects on enzymatic reactions measured *via* internal competition provide *V/K* KIEs, which report on all steps from substrate binding, up to and including the first irreversible chemical step.[25] The most valuable information for interrogating TS structure is derived from intrinsic KIEs, which reflect the chemical step alone.[26] For a given isotope x, the intrinsic KIE on an enzymatic reaction (^{x}k) can be extracted from the $^{x}V/K$

KIE using Northrop's equation (eq 1),[25] when forward commitment (C_f), reverse commitment (C_r), and the equilibrium isotope effect ($^xK_{eq}$) are known.

$$^xV/K = \frac{^xk + C_f + C_f \cdot {}^xK_{eq}}{1 + C_f + C_r} \quad (1)$$

As the Rv0091 reaction was irreversible under the conditions used to measure KIEs, C_r is assumed to be zero. As such, eq 1 is reduced to eq 2 whereby ^xk can be extracted from the $^x V/K$ KIE using C_f alone:

$$^xV/K = \frac{^xk + C_f}{1 + C_f} \quad (2)$$

The V/K and intrinsic KIEs for the hydrolysis of MTA by Rv0091 are reported in Table 2. Experimental KIEs were corrected for remote effects to provide the V/K KIEs, and intrinsic values were determined using eq 2 where C_f = 0.079. The value of C_f for Rv0091 was measured experimentally using the substrate trapping method developed by Rose,[27] as previously described (Figure S1).[6]

The primary C1′ KIE for *N*-ribosyltransferases is sensitive to atomic motion along the reaction coordinate and provides information for differentiating S_N1 and S_N2 reactions. For a fully dissociative S_N1 reaction, with complete loss of bond order to the leaving group and no participation of the incoming nucleophile at the TS, a primary 1′-^{14}C KIE near unity would be predicted.[9] For S_N1 mechanisms in which partial bond order to either the leaving group or the nucleophile is retained at the TS, 1′-^{14}C KIEs would range from 1.01 to 1.03. By contrast, primary 1′-^{14}C KIEs for associative S_N2 mechanisms range from 1.08 to 1.13. The 1′-^{14}C KIE measured for MTA hydrolysis by Rv0091 was 1.038 ± 0.005 (Table 2), which suggests either the N9 of the adenine leaving group and/or the oxygen of the nucleophilic water (Ow) retain partial bond order with the C1′ position at the TS. The primary 9-^{15}N KIE reports on the loss of C1′–N9 bond order and rehybridization of the N9 position. A value of 1.021 ± 0.007 was obtained for the primary 9-^{15}N KIE on the Rv0091 reaction (Table 2), which indicates that the C1′–N9 bond undergoes significant, but not full, loss of bond order at the TS.

The α-secondary 1′-H KIE for *N*-ribosyltransferases reports directly on changes in hybridization at the C1′ position and reflects the degree of oxocarbenium character retained by the ribose ring in the TS structure.[28] A highly dissociative TS, with considerable oxocarbenium character, will typically display 1′-^{3}H KIEs in the range of 1.06 to 1.22.[9] By contrast, an associative TS with less oxocarbenium character will display 1′-^{3}H KIE values ranging from 1.00 to 1.03. The 1′-^{3}H KIE measured for hydrolysis of MTA by Rv0091 was 1.207 ± 0.010 (Table 2), which suggests a TS structure with significant oxocarbenium character. Finally, the β-secondary 7-^{15}N KIE, which reports on the protonation state at the N7 position of adenine, was measured as 0.998 ± 0.005. Previous studies suggest that

intrinsic 7-^{15}N KIEs near unity for the MTAN reaction indicate protonation of the N7 position at the TS.[11]

Computational Models of the Rv0091 TS Structure

To investigate the mechanism of MTA hydrolysis by Rv0091, we developed a model of the Rv0091 TS structure using intrinsic KIEs as experimental boundaries for density functional theory (DFT) calculations. As there is no structural information available for the conformation of MTA bound to Rv0091, the input geometry for the TS structure search was taken from the coordinates for 5′-methylthiotubercidin bound to *E. coli* MTAN (PDB: 1NC1).[20] A family of energy-minimized TS structures was generated by constraining the C1′–N9 bond distance along the reaction coordinate as detailed below. Predicted KIEs were calculated (Gaussian 09, RB3LYP/6-31g(d) theory)[29] from the scaled vibrational frequencies of the optimized structures for MTA in the GS and at the TS. The optimized structure of MTA in the GS was generated without constraints using water as an implicit solvent (polarizable continuum model) and was identical for all KIE calculations.

Previous studies on the TS structures of MTAN variants from *E. coli*,[5] *S. pneumonia*,[6] and *N. meningitides*[7] found MTA hydrolysis proceeds through a $D_N{*}A_N$ process wherein C1′–N9 bond cleavage and C1′–Ow bond formation occur in a stepwise manner (Figure 3). Accordingly, initial efforts to model the Rv0091 TS structure considered two possible $D_N{*}A_N$ manifolds: (1) a $D_N^{\ddagger}{*}A_N$ mechanism in which cleavage of the C1′–N9 ribosidic bond to form an oxocarbenium intermediate is rate-limiting and (2) a $D_N{*}A_N^{\ddagger}$ mechanism in which the oxocarbenium intermediate is in equilibrium with MTA and nucleophilic attack of water is rate-limiting (Figure 3).

To examine the $D_N^{\ddagger}{*}A_N$ mechanism, TS structures were generated by fixing the C1′–N9 bond of MTA at increasing lengths from 1.6 to 3.0 Å in 0.2 Å increments. Predicted KIEs were calculated and TS structures yielding close matches to the intrinsic values were refined by varying the C1′–N9 bond along the reaction coordinate in 0.01 Å steps. The TS structure providing the closest match to the intrinsic KIEs was identified at a C1′–N9 distance of 2.78 Å, although this model matched only the primary 1′-^{14}C KIE within experimental error (Figure S2). The influence of charge accumulation on the leaving group was investigated by a parallel set of calculations to those detailed above in which the N7 position of adenine was protonated at the TS. Protonation at the N7 position activates the adenine for scission of the C1′–N9 bond by neutralizing negative charge build-up on the leaving group and is a common TS feature among *N*-ribosyltransferases,[10] including *E. coli*[5] and *N. meningitides*[7] MTANs. In this TS structure search, the best match to intrinsic KIEs was found at a C1′–N9 distance of 2.42 Å (Figure S3). Relative to the TS structures in which adenine was modeled as an anionic leaving group, the TS structure including N7 protonation provided a better match to intrinsic KIEs. The primary 1′-^{14}C and 9-^{15}N KIEs were well within experimental error of the intrinsic values, and the α-secondary 1′-^{3}H and β-secondary 7-^{15}N were just outside these boundaries (Figure S3).

The feasibility of a $D_N{*}A_N^{\ddagger}$ mechanism was also considered, in which the oxocarbenium intermediate is in equilibrium with MTA prior to the rate-limiting addition of water (Figure 3). For $D_N{*}A_N^{\ddagger}$ mechanisms, observed KIEs are the product of the equilibrium isotope

effect (EIE) for the first step and the KIE for the second step (Figure 3).[28] The EIEs for oxocarbenium formation were calculated for both neutral (N7 protonated) and anionic (N7 deprotonated) forms of adenine (Figure S4). Predicted KIEs were then calculated for TS structures involving nucleophilic attack of water on the oxocarbenium intermediate with C1′–Ow bond distances from 1.7 to 2.7 Å. Interestingly, the predicted 9-^{15}N EIEs for both neutral and anionic forms of adenine were within experimental error of the intrinsic KIEs (Figure S4). However, the product of the EIEs and KIEs (for the nucleophilic attack of water) did not agree with the intrinsic values for the 1′-^{14}C or 1′-^{3}H KIEs (Figure S4).

The preliminary $D_N^{\ddagger}*A_N$ model for MTA hydrolysis by Rv0091 (Figure S3) was refined through the addition of low bond order to the nucleophilic water. The TS structure providing the best match to intrinsic values (Table 2) had a C1′–N9 distance of 2.45 Å and a C1′–Ow distance of 2.70 Å (Figure 4). Interestingly, the C1′–Ow distance of 2.70 Å in this TS model is similar to the distance between the 1′ position of the aminoribitol ring and the bound active site water (2.75 Å) in the binary complex of 5′-methylthio-DADMe-immucillinA (MT-DADMe-ImmA) and *E. coli* MTAN (PDB: 1Y6Q; Figure S5).[30] The slight discrepancy between the predicted 7-^{15}N KIE and corresponding intrinsic value (Table 2) likely results from hydrogen bonding interactions with Asp220, which is predicted by homology modeling to interact with the N7 position of adenine,[31] but was not included in this TS model. This final model is most consistent with a dissociative A_ND_N TS displaying significant loss of C1′–N9 bond order, low bond order to the incoming nucleophile, and substantial oxocarbenium character of the ribosyl ring. The C1′–N9 distance of 2.45 Å corresponds to a 0.74 loss of bond order at the TS, and the nucleophilic water shares a bond order of 0.074 with C1′ (Table S1). Oxocarbenium character of the ribosyl ring at the TS is supported by a short O4′–C1′ bond (1.42 Å in MTA versus 1.27 Å at the TS), which corresponds to an increase of 0.468 in bond order relative to the GS (Table S1). In addition, natural bond orbital (NBO) analysis indicates the relative positive charge increases by 0.182 for C1′ and 0.178 for O4′ at the TS (Table S2).

Previous reports indicate the MTAN reaction for other species proceeds via highly dissociative (*E. coli*[5] and *S. pneumonia*[6]) and early (*N. meningitides*[7]) D_N*A_N transition states (Figure 3). As such, inclusion of the nucleophilic water in the Rv0091 TS model (Figure 4) distinguishes it from that of other MTAN variants, though dissociative A_ND_N mechanisms are common among *N*-ribosyltransferases.[28,32–35] A feature of note in the Rv0091 TS model is the Ow–C1′–N9 angle is 150.4° rather than the 180° (Figure 4), which would be predicted for optimal orbital overlap in a pure S_N2 reaction. Accordingly, the partial bond orders present in this model dictate a nonlinear TS for the most favorable orbital overlap. The term “nucleophile-assisted S_N1” has been invoked to describe S_N1 mechanisms in which low bond order must be included to the nucleophile in order to match predicted KIEs with experimental values.[36] As the C1′–Ow bond order is low (0.074; Table S1) in the Rv0091 TS model, it is plausible that the active site water could be preassociated in the TS structure *via* stabilizing interactions with the oxocarbenium species, but not directly participating in a concerted displacement reaction. Preassociation of a nucleophilic water within electron-reorganization distance of the C1′ reactive center is consistent with mass spectrometry experiments carried out with MT-DADMe-ImmA and *E. coli* MTAN, where the enzyme, inhibitor, and nucleophilic water remain associated in the gas phase.[37]

TS Analogues Are Picomolar Inhibitors of Rv0091

The first- and second-generation immucillins were developed as TS analogue inhibitors for *N*-ribosyltransferase reactions.[38–40] We sought to compare the electrostatics of the Rv0091 TS structure with those of 5′-methylthio-immucillinA (MT-ImmA; a first generation analogue) and MT-DADMe-ImmA (a second generation analogue; Figure 5). EPS maps extrapolated from single-point energy calculations (RB3LYP/6-31g(d) theory)[29] are presented in Figure 5 for the Rv0091 TS model, and optimized structures of MT-ImmA and MT-DADMe-ImmA. Comparison of the EPS maps reveals that the geometry and charge localization observed in the Rv0091 TS (Figure 5a) is more similar to that of MT-DADMe-ImmA (Figure 5b) than to MT-ImmA (Figure 5c). Consistent with these models, the K_i for MT-DADMe-ImmA with Rv0091 (1.5 nM) was 56-fold more potent than that of MT-ImmA (K_i = 85 nM).

DADMe-ImmA TS analogues inhibit MTAN activity in the picomolar to femtomolar range in other bacterial MTANs and display increased binding affinity when functionalized with hydrophobic groups at the C5′ position.[12,15] Crystallographic studies of DADMe-ImmA TS analogues with MTANs from *Salmonella enterica*[18] and *H. pylori*[15] revealed an elongated hydrophobic binding pocket proximal to the C5′ substituent of the bound immucillin scaffolds. Consistent with these findings, the most potent inhibition of Rv0091 was observed with DADMe-ImmA inhibitors bearing long alkyl groups at the C5′ position (Figure 6). For example, hexyl thioether **3** inhibited Rv0091 activity with a K_i of 87 pM, whereas methyl thioether **1** and butyl thioether **2** both displayed K_i values in the low nanomolar range (Figure 6).

Overall, DADMe-ImmA TS analogues inhibit Rv0091 less potently than they do other MTANs. For example, the K_i values for MT-DADMe-ImmA with *E. coli* MTAN and Rv0091 are 2 pM[31] and 1.5 nM (Figure 6), respectively. This difference in binding affinity for MT-DADMe-ImmA is anticipated from the lower catalytic activity of Rv0091 relative to *E. coli* MTAN. Catalytic rate enhancement has been correlated with the affinity of TS analogues for their enzyme targets by applying the Wolfenden approximation.[4,41,42] As such, the attenuated binding of DADMe-ImmA inhibitors with Rv0091 is consistent with the slow turnover of Rv0091 indicated by k_{cat}. In addition, the DADMe-ImmA scaffold was designed to mimic *N*-ribosyltransferase reactions with highly dissociative TS structures.[38–40] The crystal structure of MT-DADMe-ImmA in binary complex with *E. coli* MTAN reveals a distance of 2.8 Å between the N1′ position of the 3′-hydroxypyrrolidine ring and C9 of the 9-deazaadenine moiety.[30] This inhibitor geometry is a good match to the TS structure of *E. coli* MTAN wherein adenine is 3.0 Å from C1′.[31] By comparison, the Rv0091 TS structure is somewhat earlier with a C1′–N9 distance of 2.45 Å (Figure 4). Moreover, the protonated aminoribitol scaffold of the DADMe-ImmA analogues (Figure 6) is designed to mimic the oxocarbenium species resulting from near full dissociation of adenine. The earlier TS of Rv0091 (relative to *E. coli* MTAN) would result in less electropositive charge at the C1′ position, which may not be as accurately mimicked by the DADMe-ImmA scaffold. The EPS maps for the Rv0091 TS structure (Figure 5a) and MT-DADMe-ImmA (Figure 5b) reveal greater positive charge is localized at the 1′ position of the inhibitor. Accordingly, differences in TS geometry and electrostatics between *E. coli*

MTAN and Rv0091 may also contribute to the lower potency observed for DADMe-ImmA inhibitors with the Rv0091 protein.

The TDR *M. tuberculosis* gene function library classifies Rv0091 as a nonessential gene.[45,46] This is consistent with the assignment of Rv0091 as a putative MTAN with roles in quorum sensing and SAM recycling. With the function of Rv0091 now defined as a 5′-dAdo hydrolase, the *in vivo* activity of Rv0091 is more likely coupled to radical SAM reactions that act to generate radical reaction centers, with 5′-dAdo and methionine as products. Radical SAM enzymes are recognized by the CX_3CX_2C motif,[47] and 21 of these proteins have been annotated in the *M. tuberculosis* genome.[48] Preliminary growth experiments with *M. tuberculosis* indicate that MT-DADMe-ImmA (**3**) and butylthio-DADMe-immucillinA (**4**) have no effect on growth of cultured cells.

CONCLUSION

The Rv0091 protein from *M. tuberculosis*, previously annotated as a putative MTAN, exists as a dimer in solution and displays substrate specificity for 5′-dAdo relative to MTA and SAH. Thus, the protein is not crucial in quorum sensing pathways but more likely plays a role in reactions involving SAM radical enzymes. Intrinsic KIE measurements and quantum chemical calculations were used to establish a model for the TS structure of Rv0091. The TS for Rv0091 differs from the transition states of previously reported MTANs. The Rv0091 TS is characterized by a significant decrease in C1′–N9 bond order, substantial oxocarbenium character of the ribosyl ring, and weak participation of the water nucleophile. DADMe-ImmA TS analogues resemble the Rv0091 TS structure and inhibit Rv0091 activity with K_i values in the range of 10^{-9} to 10^{-11} M. The most potent inhibitor of Rv0091 activity identified in this study was hexyl-thio-DADMe-immucillinA, which exhibited a K_i of 87 pM. Studies to investigate the *in vivo* role of Rv0091 in mycobacteria, as well as the potential for DADMe-ImmA TS analogues to function as modulators of virulence in *M. tuberculosis*, are ongoing.

METHODS

Full details for all experimental methods are provided in the Supporting Information.

Supplementary Material

Refer to Web version on PubMed Central for supplementary material.

Acknowledgments

We thank M. Poulin (Einstein), Z. Wang (Einstein), and A. Gizzi (Einstein) for helpful discussions. The inhibitor molecules were a generous gift of P. C. Tyler and G. B. Evans from the Ferrier Research Institute, Victoria University of Wellington, New Zealand. This work was supported by research grant GM041916 and training grant T32AI070117 from the National Institutes of Health.

References

1. World Health Organization. WHO global tuberculosis report. World Health Organization; Geneva, Switzerland: 2015.

2. CDC - Tuberculosis (TB). http://www.cdc.gov/tb/
3. Parveen N, Cornell KA. Methylthioadenosine/S-adenosylhomocysteine nucleosidase, a critical enzyme for bacterial metabolism. Mol. Microbiol. 2011; 79:7–20. [PubMed: 21166890]
4. Schramm VL. Enzymatic transition states, transition-state analogs, dynamics, thermodynamics, and lifetimes. Annu. Rev. Biochem. 2011; 80:703–732. [PubMed: 21675920]
5. Singh V, Lee JE, Nunez S, Howell PL, Schramm VL. Transition state structure of 5′-methylthioadenosine/S-adenosylhomocysteine nucleosidase from Escherichia coli and its similarity to transition state analogues. Biochemistry. 2005; 44:11647–11659. [PubMed: 16128565]
6. Singh V, Schramm VL. Transition-state analysis of S. pneumoniae 5′-methylthioadenosine nucleosidase. J. Am. Chem. Soc. 2007; 129:2783–2795. [PubMed: 17298059]
7. Singh V, Luo M, Brown RL, Norris GE, Schramm VL. Transition-state structure of neisseria meningitides 5′-methylthioadenosine/S-adenosylhomocysteine nucleosidase. J. Chem. Soc. 2007; 129:13831–13833.
8. Schramm VL. Enzymatic transition state theory and transition state analogue design. J. Biol. Chem. 2007; 282:28297–28300. [PubMed: 17690091]
9. Schramm VL. Enzymatic transition states and transition state analog design. Annu. Rev. Biochem. 1998; 67:693–720. [PubMed: 9759501]
10. Schramm VL. Enzymatic transition-state analysis and transition-state analogs. Methods Enzymol. 1999; 308:301–355. [PubMed: 10507010]
11. Singh V, Shi W, Almo SC, Evans GB, Furneaux RH, Tyler PC, Painter GF, Lenz DH, Mee S, Zheng R, Schramm VL. Structure and inhibition of a quorum sensing target from Streptococcus pneumoniae. Biochemistry. 2006; 45:12929–12941. [PubMed: 17059210]
12. Gutierrez JA, Luo M, Singh V, Li L, Brown RL, Norris GE, Evans GB, Furneaux RH, Tyler PC, Painter GF, Lenz DH, Schramm VL. Picomolar inhibitors as transition-state probes of 5′-methylthioadenosine nucleosidases. ACS Chem. Biol. 2007; 2:725–734. [PubMed: 18030989]
13. Schramm VL. Enzymatic transition states and transition state analogues. Curr. Opin. Struct. Biol. 2005; 15:604–613. [PubMed: 16274984]
14. Gutierrez JA, Crowder T, Rinaldo-Matthis A, Ho MC, Almo SC, Schramm VL. Transition state analogs of 5′-methylthioadenosine nucleosidase disrupt quorum sensing. Nat. Chem. Biol. 2009; 5:251–257. [PubMed: 19270684]
15. Wang S, Cameron SA, Clinch K, Evans GB, Wu Z, Schramm VL, Tyler PC. New Antibiotic Candidates against Helicobacter pylori. J. Am. Chem. Soc. 2015; 137:14275–14280. [PubMed: 26494017]
16. de Souza GA, Leversen NA, Malen H, Wiker HG. Bacterial proteins with cleaved or uncleaved signal peptides of the general secretory pathway. J. Proteomics. 2011; 75:502–510. [PubMed: 21920479]
17. Payne JW. Polymerization of proteins with glutaraldehyde. Soluble molecular-weight markers. Biochem. J. 1973; 135:867–873. [PubMed: 4204954]
18. Haapalainen AM, Thomas K, Tyler PC, Evans GB, Almo SC, Schramm VL. Salmonella enterica MTAN at 1.36 A resolution: a structure-based design of tailored transition state analogs. Structure. 2013; 21:963–974. [PubMed: 23685211]
19. Ronning DR, Iacopelli NM, Mishra V. Enzyme-ligand interactions that drive active site rearrangements in the Helicobacter pylori 5′-methylthioadenosine/S-adenosylhomocysteine nucleosidase. Protein Sci. 2010; 19:2498–2510. [PubMed: 20954236]
20. Lee JE, Cornell KA, Riscoe MK, Howell PL. Structure of Escherichia coli 5′-methylthioadenosine/S-adenosylhomocysteine nucleosidase inhibitor complexes provide insight into the conformational changes required for substrate binding and catalysis. J. Biol. Chem. 2003; 278:8761–8770. [PubMed: 12496243]
21. Buckoreelall K, Sun Y, Hobrath JV, Wilson L, Parker WB. Identification of Rv0535 as methylthioadenosine phosphorylase from Mycobacterium tuberculosis. Tuberculosis (Oxford, U. K.). 2012; 92:139–147.
22. Buckoreelall K, Wilson L, Parker WB. Identification and characterization of two adenosine phosphorylase activities in Mycobacterium smegmatis. J. Bacteriol. 2011; 193:5668–5674. [PubMed: 21821769]

23. Thomas K, Cameron SA, Almo SC, Burgos ES, Gulab SA, Schramm VL. Active site and remote contributions to catalysis in methylthioadenosine nucleosidases. Biochemistry. 2015; 54:2520–2529. [PubMed: 25806409]
24. Banerjee S, Agrawal MJ, Mishra D, Sharan S, Balaram H, Savithri HS, Murthy MR. Structural and kinetic studies on adenylosuccinate lyase from Mycobacterium smegmatis and Mycobacterium tuberculosis provide new insights on the catalytic residues of the enzyme. FEBS J. 2014; 281:1642–1658. [PubMed: 24479855]
25. Northrop DB. The expression of isotope effects on enzyme-catalyzed reactions. Annu. Rev. Biochem. 1981; 50:103–131. [PubMed: 7023356]
26. Cleland WW. The use of isotope effects to determine transition-state structure for enzymic reactions. Methods Enzymol. 1982; 87:625–641. [PubMed: 7176928]
27. Rose IA. The isotope trapping method: desorption rates of productive E.S complexes. Methods Enzymol. 1980; 64:47–59. [PubMed: 7374457]
28. Berti PJ, Tanaka KSE. Transition State Analysis Using Multiple Kinetic Isotope Effects: Mechanisms of Enzymatic and Non-enzymatic Glycoside Hydrolysis and Transfer. Adv. Phys. Org. Chem. 2002; 37:239–314.
29. Frisch, MJ., Trucks, GW., Schlegel, HB., Scuseria, GE., Robb, MA., Cheeseman, JR., Scalmani, G., Barone, V., Mennucci, B., Petersson, GA., Nakatsuji, H., Caricato, M., Li, X., Hratchian, HP., Izmaylov, AF., Bloino, J., Zheng, G., Sonnenberg, JL., Hada, M., Ehara, M., Toyota, K., Fukuda, R., Hasegawa, J., Ishida, M., Nakajima, TE., Honda, Y., Kitao, O., Nakai, H., Vreven, T., Montgomery, JA., Peralta, JE., Ogliaro, F., Bearpark, M., Heyd, JJ., Brothers, E., Kudin, KN., Staroverov, VN., Kobayashi, R., Normand, J., Raghavachari, K., Rendell, A., Burant, JC., Iyengar, SS., Tomasi, J., Cossi, M., Rega, N., Millam, JM., Klene, M., Knox, JE., Cross, JB., Bakken, V., Adamo, C., Jaramillo, J., Gomperts, R., Stratmann, RE., Yazyev, O., Austin, AJ., Cammi, R., Pomelli, C., Ochterski, JW., Martin, RL., Morokuma, K., Zakrzewski, VG., Voth, GA., Salvador, P., Dannenberg, JJ., Dapprich, S., Daniels, AD., Farkas, Ö., Foresman, JB., Ortiz, JV., Cioslowski, J., Fox, DJ. Gaussian 09. Gaussian, Inc; Wallingford, CT: 2009.
30. Lee JE, Singh V, Evans GB, Tyler PC, Furneaux RH, Cornell KA, Riscoe MK, Schramm VL, Howell PL. Structural rationale for the affinity of pico- and femtomolar transition state analogues of Escherichia coli 5′-methylthioadenosine/S-adenosylhomocysteine nucleosidase. J. Biol. Chem. 2005; 280:18274–18282. [PubMed: 15746096]
31. Singh V, Evans GB, Lenz DH, Mason JM, Clinch K, Mee S, Painter GF, Tyler PC, Furneaux RH, Lee JE, Howell PL, Schramm VL. Femtomolar transition state analogue inhibitors of 5′-methylthioadenosine/S-adenosylhomocysteine nucleosidase from Escherichia coli. J. Biol. Chem. 2005; 280:18265–18273. [PubMed: 15749708]
32. Bates C, Kendrick Z, McDonald N, Kline PC. Transition state analysis of adenosine nucleosidase from yellow lupin (Lupinus luteus). Phytochemistry. 2006; 67:5–12. [PubMed: 16300810]
33. Berti PJ, McCann JA. Toward a detailed understanding of base excision repair enzymes: transition state and mechanistic analyses of N-glycoside hydrolysis and N-glycoside transfer. Chem. Rev. 2006; 106:506–555. [PubMed: 16464017]
34. Kline PC, Schramm VL. Purine nucleoside phosphorylase. Catalytic mechanism and transition-state analysis of the arsenolysis reaction. Biochemistry. 1993; 32:13212–13219. [PubMed: 8241176]
35. Schwartz PA, Vetticatt MJ, Schramm VL. Transition state analysis of the arsenolytic depyrimidination of thymidine by human thymidine phosphorylase. Biochemistry. 2011; 50:1412–1420. [PubMed: 21222488]
36. Gawlita E, Szylhabel-Godala A, Paneth P. Kinetic Isotope Effects on the Menshutkin Reaction: Theory Versus Experiment. J. Phys. Org. Chem. 1996; 9:41–49.
37. Wang S, Lim J, Thomas K, Yan F, Angeletti RH, Schramm VL. A complex of methylthioadenosine/S-adenosylhomocysteine nucleosidase, transition state analogue, and nucleophilic water identified by mass spectrometry. J. Am. Chem. Soc. 2012; 134:1468–1470. [PubMed: 22239413]
38. Evans GB, Furneaux RH, Lewandowicz A, Schramm VL, Tyler PC. Synthesis of second-generation transition state analogues of human purine nucleoside phosphorylase. J. Med. Chem. 2003; 46:5271–5276. [PubMed: 14613329]

39. Furneaux RH, Limberg G, Tyler PC, Schramm VL. Synthesis of transition state inhibitors for N-riboside hydrolases and transferases. Tetrahedron. 1997; 53:2915–2930.
40. Evans GB, Furneaux RH, Gainsford GJ, Schramm VL, Tyler PC. Synthesis of transition state analogue inhibitors for purine nucleoside phosphorylase and N-riboside hydrolases. Tetrahedron. 2000; 56:3053–3062.
41. Wolfenden R. Transition state analogues for enzyme catalysis. Nature. 1969; 223:704–705. [PubMed: 4979456]
42. Wolfenden R, Snider MJ. The depth of chemical time and the power of enzymes as catalysts. Acc. Chem. Res. 2001; 34:938–945. [PubMed: 11747411]
43. Thomas K, Haapalainen AM, Burgos ES, Evans GB, Tyler PC, Gulab S, Guan R, Schramm VL. Femtomolar inhibitors bind to 5′-methylthioadenosine nucleosidases with favorable enthalpy and entropy. Biochemistry. 2012; 51:7541–7550. [PubMed: 22931458]
44. Copeland, RA. Enzymes. 2. Wiley; Canada: 2000.
45. TDR Targets. http://tdrtargets.org
46. Sassetti CM, Rubin EJ. Genetic requirements for mycobacterial survival during infection. Proc. Natl. Acad. Sci. U. S. A. 2003; 100:12989–12994. [PubMed: 14569030]
47. Sofia HJ, Chen G, Hetzler BG, Reyes-Spindola JF, Miller NE. Radical SAM, a novel protein superfamily linking unresolved steps in familiar biosynthetic pathways with radical mechanisms: functional characterization using new analysis and information visualization methods. Nucleic Acids Res. 2001; 29:1097–1106. [PubMed: 11222759]
48. Akiva E, Brown S, Almonacid DE, Barber AE 2nd, Custer AF, Hicks MA, Huang CC, Lauck F, Mashiyama ST, Meng EC, Mischel D, Morris JH, Ojha S, Schnoes AM, Stryke D, Yunes JM, Ferrin TE, Holliday GL, Babbitt PC. The Structure-Function Linkage Database. Nucleic Acids Res. 2014; 42:D521–530. [PubMed: 24271399]

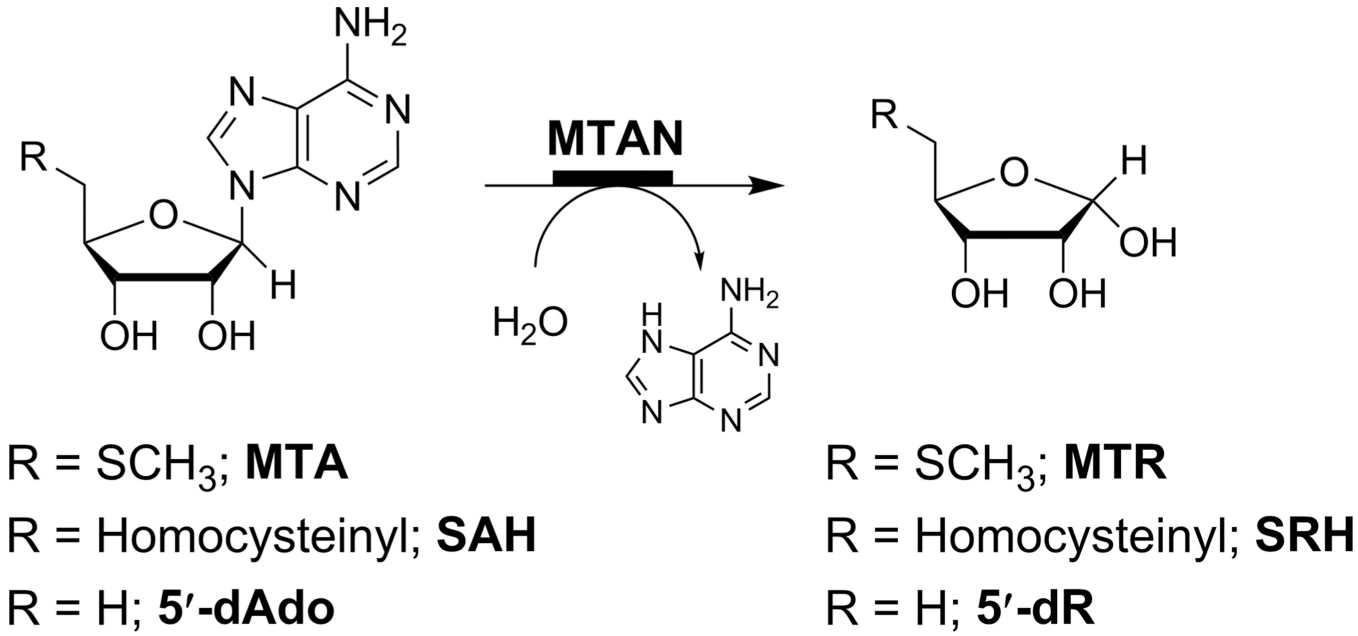

Figure 1.

The MTAN reaction. MTANs catalyze the hydrolysis of the *N*-ribosidic bond of 5′-methylthioadenosine (MTA), *S*-adenosylhomocysteine (SAH), and 5′-deoxyadenosine (5′-dAdo) to produce methylthioribose (MTR), *S*-ribosylhomocysteine (SRH), and 5′-deoxyribose (5′-dR), respectively. MTAN: 5′-methylthioadenosine nucleosidase.

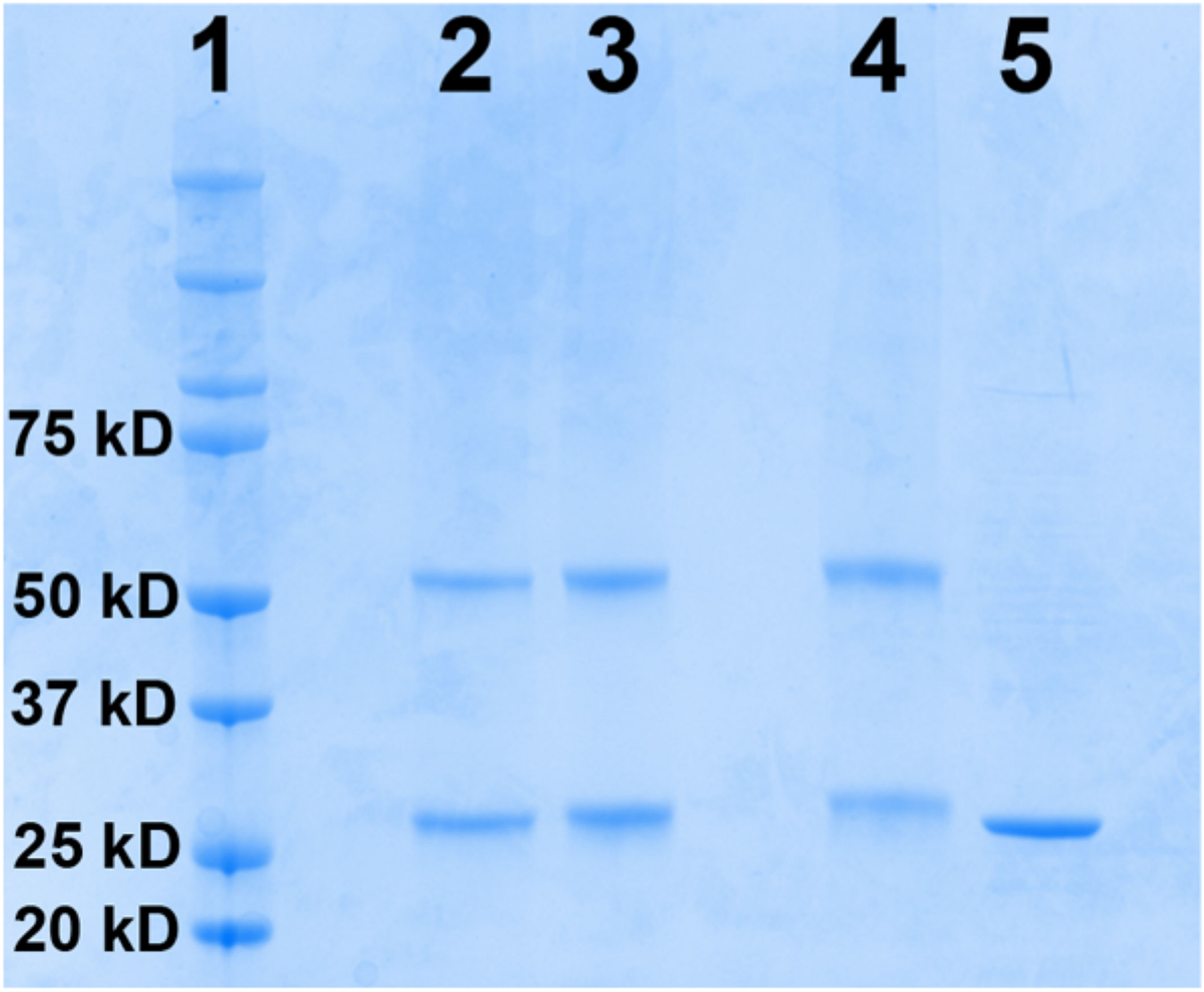

Figure 2.

SDS-PAGE analysis of purified monomeric and cross-linked Rv0091. Rv0091 was purified to homogeneity, and SDS-PAGE analysis revealed a band consistent with the predicted mass (29.4 kDa) of the monomeric protein. The pure protein was treated with 0.1% to 2% glutaraldehyde to allow for intersubunit cross-linking. A band consistent with a dimeric oligomerization state was observed for the cross-linked protein. Lane 1, protein molecular weight standards; lane 2, Rv0091 + 0.1% glutaraldehyde; lane 3, Rv0091 + 0.5% glutaraldehyde; lane 4, Rv0091 + 2% glutaraldehyde; lane 5, Rv0091 before cross-linking.

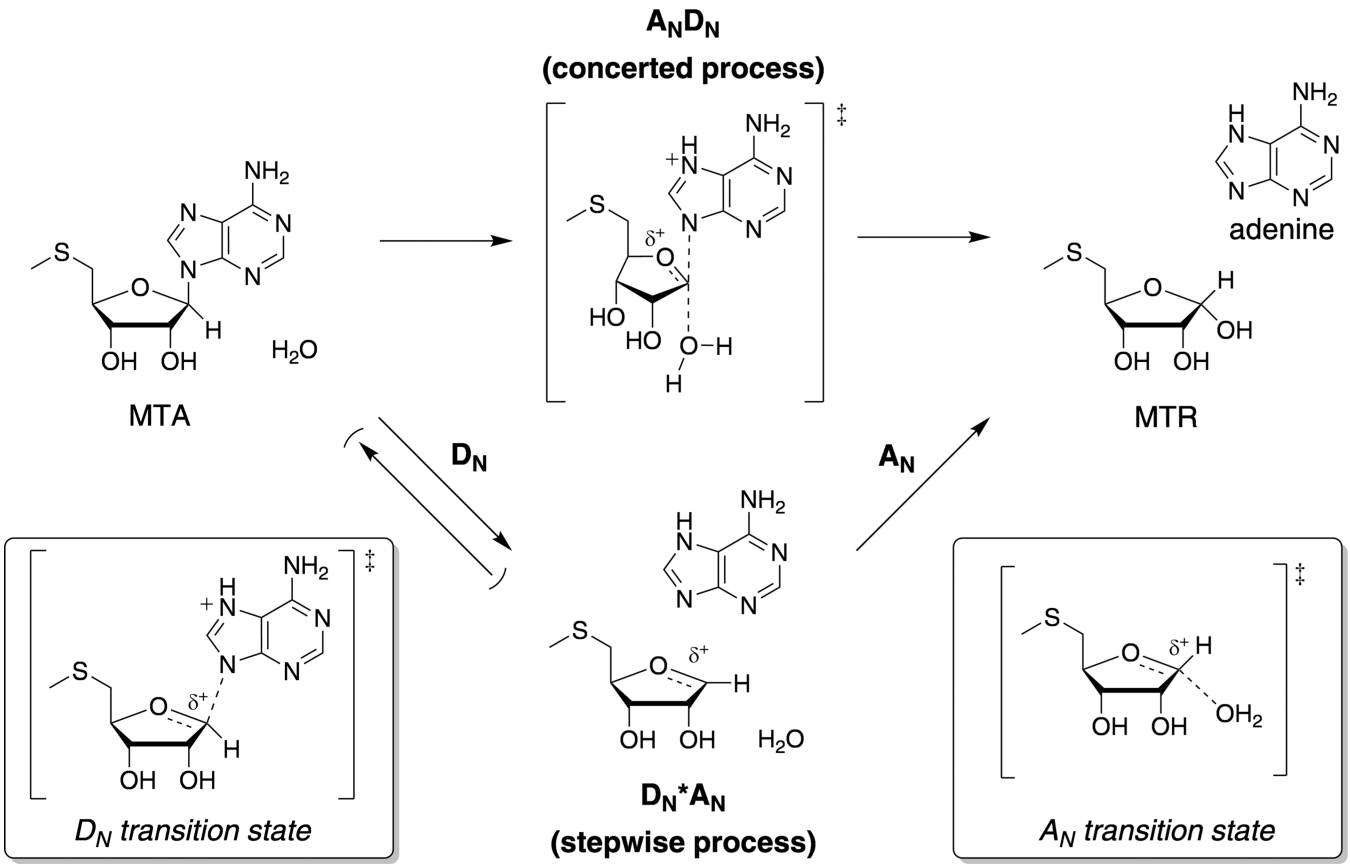

Figure 3.

General mechanisms for the hydrolysis of MTA by Rv0091. The Rv0091 reaction is represented as two possible mechanisms in which the transformations are considered as their elementary steps. For MTA hydrolysis, the A_N step refers to the association of the water nucleophile and the D_N step refers to dissociation of the adenine leaving group. If the reaction proceeds through a concerted bimolecular TS, the mechanism is termed A_ND_N. If dissociation of the leaving group precedes association of the nucleophile and the reaction proceeds through a stepwise process *via* discrete transition states, the reaction is termed $D_N{*}A_N$. For $D_N{*}A_N$ processes, a superscript "‡" is used to denote the rate-limiting step, *e.g.,* $D_N{}^{‡}{*}A_N$ or $D_N{*}A_N{}^{‡}$. MTA, 5′-methylthioadenosine; MTR, 5′-methylthioribose.

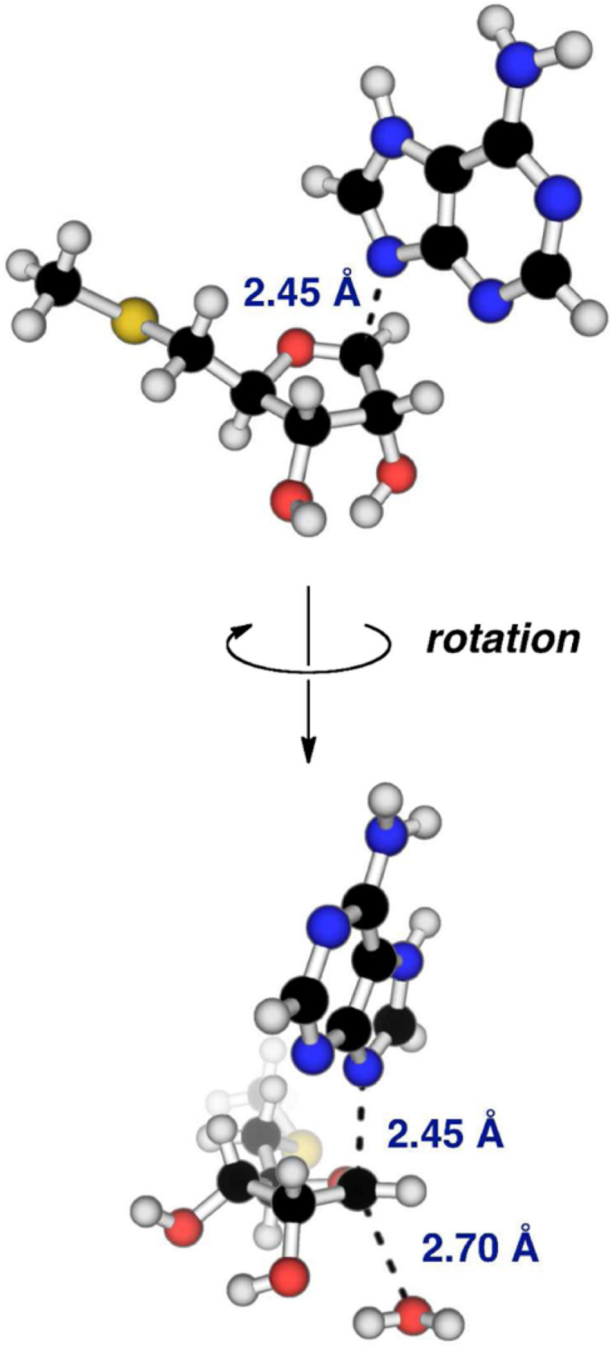

Figure 4.

Calculated model for the Rv0091 TS structure. TS structure model of MTA hydrolysis catalyzed by Rv0091 was generated by matching KIEs predicted for calculated transition states (RB3LYP/6-31g(d) theory) to intrinsic KIEs. Features of the Rv0091 TS structure include a C1′–N9 bond distance of 2.45 Å, a C1′–Ow bond distance of 2.70 Å, protonation at the N7 position of adenine, and significant oxocarbenium character. TS, transition state; MTA, 5′-methylthioadenosine; KIEs, kinetic isotope effects; Ow, water.

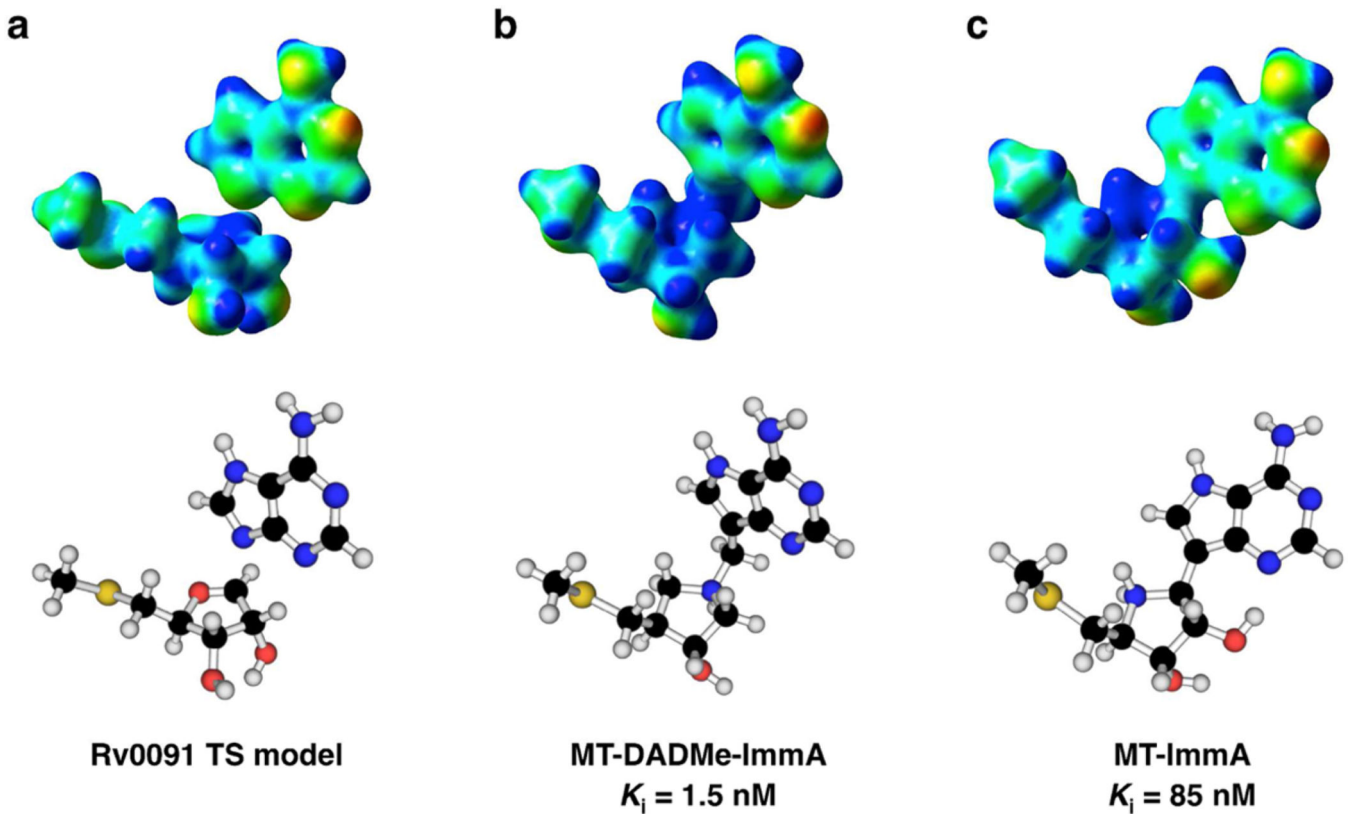

Figure 5.

EPS maps for Rv0091 TS structure and immucillin TS analogues. EPS maps (red = partial negative; blue = partial positive) were extrapolated from single-point energy calculations (RB3LYP/6-31g(d) theory)[29] and visualized in GaussView 5.0 (isovalue = 0.04). (a) Energy-minimized structure and EPS map for the TS structure of MTA hydrolysis by Rv0091. (b) Energy-minimized structure and EPS map for MTDADMe-ImmA. (c) Energy-minimized structure and EPS map for MT-ImmA. EPS, electrostatic potential surface; TS, transition state; MTA, 5′-methylthioadenosine; MT-DADMe-ImmA, 5′-methylthio-DADMe-immucillinA; MT-ImmA, 5′-methylthioimmucillin-A.

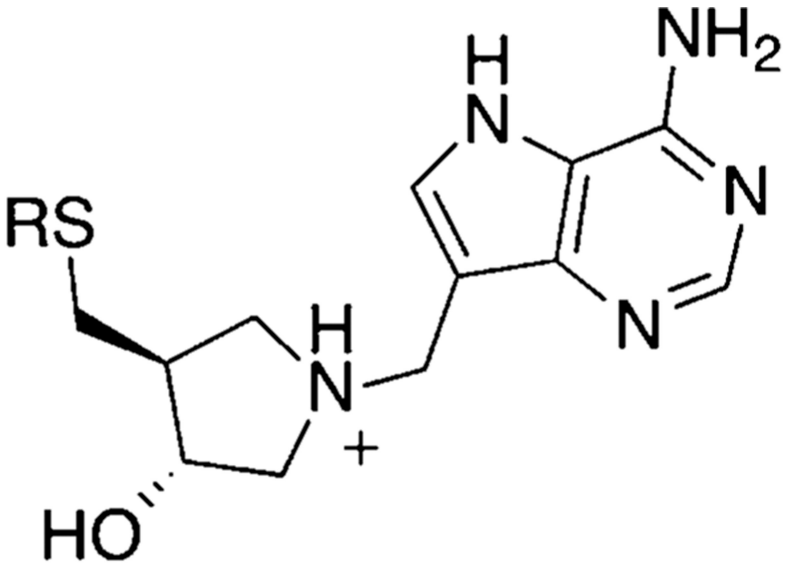

	R =	K_i (nM)
1	Methyl	1.5 ± 0.4
2	*n*-Butyl	1.3 ± 0.1
3	*n*-Hexyl	0.087 ± 0.012
4	2-(R/S) Ethylhex-1-yl	0.099 ± 0.009
5	*p*-Chlorophenyl	0.258 ± 0.013
6	4-Hydroxybutyl	0.606 ± 0.07

Figure 6.

Inhibition of Rv0091 with DADMe-ImmA TS analogues. Inhibition of Rv0091 activity was monitored at 305 nm *via* a coupled assay with xanthine oxidase[43] in which the adenine product was converted to 2,8-dihydroxyadenine. The K_i values were calculated using the Morrison equation for tight-binding inhibitors.[44]

Table 1

Kinetic Parameters for Rv0091 with 5′-dAdo, MTA, and SAH[a]

substrate[b]	k_{cat} (s^{-1})	K_M (μM)	k_{cat}/K_M (M^{-1} s^{-1})
5′-dAdo	0.47 ± 0.02	10.9 ± 1.5	43.4×10^3
MTA	0.023 ± 0.001	3.7 ± 0.4	6.3×10^3
SAH	0.004 ± 0.001	63.1 ± 7.0	0.06×10^3

[a]Parameters obtained using a luciferase-based assay[23] at 25 °C.

[b]Adenosine and 2′-deoxyadenosine showed less substrate activity than MTA and were not further characterized.

5′-dAdo, 5′-deoxyadenosine; MTA, 5′-methylthioadenosine; SAH, *S*-adenosylhomocysteine.

Table 2

Kinetic Isotope Effects for the Hydrolysis of MTA by Rv0091

heavy MTA	light MTA	type of KIE	*V/K* KIEs	intrinsic KIEs[c]	calculated KIEs[d]
[1′-^{14}C]	[5′-$^{3}H_2$]	primary	1.035 ± 0.004[b]	1.038 ± 0.005	1.039
[1′-^{3}H]	[5′-^{14}C][a]	*α*-secondary	1.194 ± 0.009	1.207 ± 0.010	1.209
[9-^{15}N, 5′-^{14}C]	[5′-$^{3}H_2$]	primary	1.019 ± 0.006[b]	1.021 ± 0.007	1.023
[7-^{15}N, 5′-^{14}C]	[5′-$^{3}H_2$]	*β*-secondary	0.998 ± 0.004[b]	0.998 ± 0.005	0.985
[5′-$^{3}H_2$]	[5′-^{14}C]	remote	0.998 ± 0.008	0.998 ± 0.009	0.990

[a] The KIE on the remote [5′-^{14}C] label is assumed to be unity.

[b] Experimental values were corrected for the remote [5′-$^{3}H_2$] KIE using the expression $KIE = KIE_{obs} \times [5'\text{-}^{3}H_2]\ KIE$.

[c] Intrinsic KIEs were determined by correcting *V/K* values using eq 2 assuming $C_f = 0.079$.

[d] Calculated values (Gaussian 09, RB3LYP/6-31g(d) theory) corresponds to those for the final TS model shown in Figure 4.